

Equivalent Circuit Modeling and Parameter Identification for Lithium-ion Batteries Based on Improved Barnacle Mating Optimizer

Jiarong Li,¹ Cheng-Jian Lin,^{2,3*} Haiyu Wang,⁴ and Jiarong Kan¹

¹College of Electrical Engineering, Yancheng Institute of Technology, Jiangsu 224000, China

²Department of Computer Science and Information Engineering, National Chin-Yi University of Technology,
Taichung 41170, Taiwan

³College of Intelligence, National Taichung University of Science and Technology, Taichung 404, Taiwan

⁴State Key Laboratory of Reliability and Intelligence of Electrical Equipment,
Key Laboratory of Electromagnetic Field and Electrical Apparatus Reliability of Hebei Province,
Hebei University of Technology, Tianjin 300401, China

(Received July 4, 2022; accepted September 13, 2022)

Keywords: evolutionary computation, parameter identification, barnacle mating optimizer, lithium-ion battery, electric vehicles

To address the current problems of accuracy and reliability of the equivalent circuit models for lithium-ion batteries and sensors, in this study we propose an improved barnacle mating optimizer (IBMO) to accurately identify parameters. First, an improved second-order RC model (ISO RC) is derived by segmenting the battery hysteresis voltage and introducing it into the second-order RC model (SO RC model) as a controlled source, which better reflects the dynamic effects of the battery than the SO RC model. Second, the tent chaos mapping, cosine control factor, and Levy flight strategy are introduced to enhance the convergence performance of the IBMO. Its convergence performance is verified by comparison with other existing intelligent algorithms using five single-peak and four multi-peak test functions. Finally, the IBMO-ISO RC model is established by using the IBMO as the identification strategy of the ISO RC model in the simulation of two real operating conditions of lithium-ion batteries. The root mean square error of the model under the two operating conditions is only 0.0431 and 0.0483, and the mean absolute percentage error is only 0.38 and 0.56%, outperforming other existing models. The IBMO proposed in this study enables higher model recognition accuracy, making it highly convenient for lithium-ion battery and sensor-related research.

1. Introduction

Behind the increasing application of lithium-ion batteries (LIBs) and sensors, the related technologies based on their application have also received increasing attention from many researchers.⁽¹⁾ Li *et al.*⁽²⁾ argued that battery and sensor modeling technology can simulate static and dynamic behaviors and is a fundamental technology for conducting sensor- and LIB-related research. Zhao *et al.*⁽³⁾ claimed that accurate models can simulate the actual operating conditions

*Corresponding author: e-mail: cjlin@ncut.edu.tw
<https://doi.org/10.18494/SAM4027>

of batteries, making them highly convenient for LIB-related research and promoting the development of new energy grid-connected power generation and green transportation and the alleviation of the shortage of traditional energy sources and the problem of environmental pollution.

Currently, the most commonly used battery model is the equivalent circuit model (ECM).⁽⁴⁾ The ECM simulates the external characteristics of a real battery by forming a two-port network with ideal power supplies, capacitors, and other components.⁽⁵⁾ The ECM structure is relatively simple, its accuracy is high, and it can be built relatively easily in various circuit simulation software, resulting in its frequent application. Kalogiannis *et al.*⁽⁶⁾ argued that the accuracy of the ECM is influenced by various factors. First, the ability to correctly simulate the dynamic/static response of the battery is an important indicator for judging the accuracy of the model. The second-order RC model (SO RC model) simulates the electrochemical polarization reaction and the concentration difference polarization reaction of the battery separately, which can effectively reflect the dynamic characteristics of the battery, but it fails to consider its hysteresis effect.⁽⁷⁾ Therefore, in this study we propose a correction strategy based on the previous work to balance the hysteresis effect, thus improving the accuracy of the model.

Ouyang *et al.*⁽⁸⁾ argued that the model identification strategy also has a significant impact on the simulation accuracy of battery and sensor models. Numerous scholars have proposed parameter identification strategies based on the many available intelligent optimization algorithms.⁽⁹⁾ Such methods can quickly and accurately identify the model parameters of LIBs and sensors by virtue of the optimization-seeking capability of intelligent algorithms.⁽¹⁰⁾ The barnacle mating optimizer (BMO) is a novel heuristic algorithm for the optimization of complex problems.⁽¹¹⁾ It has the advantages of few parameters, high merit-seeking ability, and a simple principle. However, it has some drawbacks, including insufficient population diversity at the beginning of iteration, falling easily into a local optimum, and unstable convergence performance. In this study, an improved barnacle mating optimizer (IBMO) based on the BMO is proposed to effectively solve its shortcomings and apply it to the problem of LIB parameter identification. The IBMO has better convergence accuracy and convergence speed than comparative algorithms and can accurately and effectively identify the parameters of LIB models.

The main contributions of this study are as follows.

- (1) We propose an ECM model for LIBs that considers the hysteresis effect, called the improved SO RC model (ISO RC model), which has improved accuracy compared with SO RC.
- (2) An IBMO with strong convergence performance is proposed to identify the parameters of LIB models.
- (3) The parameter identification accuracy of the IBMO was verified for two actual battery operating conditions.

The remainder of this study is organized as follows: Sect. 2 introduces studies related to the parameter identification problem of LIBs; Sect. 3 describes the process of establishing the ISO RC model; Sect. 4 introduces the proposed IBMO and verifies its performance; Sect. 5 presents the simulation of the IBMO-ISO RC model for two types of batteries with actual operating conditions; Sect. 6 summarizes the research and its contributions and provides an outlook on future research.

2. Literature Review

The problem of LIB model parameter identification has received much attention because of its importance in research related to LIBs.⁽¹²⁾ Previous studies have focused on two aspects. The first is to improve the ECM to increase its accuracy and adaptability. The other is to investigate the model identification strategy to better exploit the advantages of the model.

The key point in improving the ECM is to simulate the hysteresis effect with higher accuracy. The most direct way to simulate the hysteresis effect is to use the average open circuit voltage (OCV) curves of the battery charge and discharge as the OCV curves of the model, but this method can cause large hysteresis errors in the model in the case of complex battery conditions.⁽¹³⁾ Plett⁽¹⁴⁾ proposed an improved model that fitted the hysteresis effect as a function of state of charge (SOC) and time. The method improves the accuracy of the model but increases its complexity, making the operation substantially slower. Windarko and Choi⁽¹⁵⁾ modeled the hysteresis by mapping the input and output of the primary and secondary hysteresis loops, which provides some control over the hysteresis error. However, the model generated by this method cannot describe the secondary hysteresis loop. Therefore, the accuracy of the model cannot be further improved.

Model parameter identification strategies are mainly divided into online and offline identification. Online identification can modify the model parameters in real time in accordance with the working environment of the model, making it suitable for real-time control of the battery, but it requires a high computing speed of the processor. Verbrugge and Koch⁽¹⁶⁾ and Pattipati *et al.*⁽¹⁷⁾ improved the basis of the least squares (LS) method and proposed a weighted regression LS method and a recursive LS method based on the forgetting factor, respectively, to achieve the real-time estimation of parameters. However, these two methods generate large measurement noise as the amount of cell data increases, thus significantly reducing the discrimination accuracy. Tan *et al.*⁽¹⁸⁾ combined the recursive LS method and the extended Kalman filter algorithm, thereby combining the advantages of the two methods and significantly improving the discrimination accuracy, but this increased the complexity of the model and was not applicable to system-level operations. Traditional offline identification methods mainly include the LS method and subspace method.⁽¹⁹⁾ These methods are more direct and simpler, but the recognition accuracy is low. However, with the application of heuristic algorithms in the field of battery parameter identification, the accuracy and reliability of offline identification strategies have substantially improved. Shen and Li⁽²⁰⁾ proposed a multiscale parameter identification method that combines the particle swarm optimization algorithm (PSO) and the Levenberg–Marquardt algorithm (LM), with PSO used for coarse-scale identification and LM used for fine-scale identification, thus effectively improving the convergence accuracy of the algorithm. However, this increased the complexity of the model and reduced its convergence speed. Yu *et al.*⁽²¹⁾ and Li *et al.*⁽²²⁾ improved PSO by proposing the co-evolutionary PSO and the mixed-swarm-based cooperative PSO, respectively, which improved the convergence performance and robustness of the algorithm and increased the identification accuracy. El-Sehiemy *et al.*⁽²³⁾ and Ferahtia *et al.*⁽²⁴⁾ used an enhanced sunflower optimization algorithm and the artificial ecosystem optimization algorithm, respectively, for parameter identification modeling, which

improved the speed of model identification and the efficiency of the parameter identification process. However, the above algorithms still have convergence problems, and the identification model still has some limitations and cannot maintain stable identification accuracy under the varying working conditions of the battery environment.

In this study, an IBMO-ISO RC parameter identification strategy is proposed. The strategy considers the hysteresis effect, and the convergence performance of the algorithm is improved by adding tent chaos mapping, the cosine control factor, and Levy flight strategy to the identification strategy. The proposed strategy has high identification accuracy, and its accuracy and adaptability are verified for two different working conditions.

3. Lithium-ion Battery Equivalence Model

3.1 SO RC model

The SO RC model decomposes the polarization effect into an electrochemical polarization effect and a concentration difference polarization effect, which are each represented by an RC resistance network, to cope with complex cell operating conditions, as shown in Fig. 1. Here, R_{pa} and R_{pb} denote the electrochemical polarization resistance and the concentration polarization resistance, and C_{pa} and C_{pb} denote the electrochemical polarization capacitance and the concentration polarization capacitance, respectively.

The terminated voltage equation is expressed as

$$U_t = U_{ocv}(soc) - R \cdot i_L - U_{pa} - U_{pb}, \quad (1)$$

$$U_{pa}^{j+1} = U_{pa}^j \cdot e^{-\frac{\Delta t}{\tau_1}} + i_L^j \cdot (1 - e^{-\frac{\Delta t}{\tau_1}}) \cdot R_{pa}, \quad (2)$$

$$U_{pb}^{j+1} = U_{pb}^j \cdot e^{-\frac{\Delta t}{\tau_2}} + i_L^j \cdot (1 - e^{-\frac{\Delta t}{\tau_2}}) \cdot R_{pb}, \quad (3)$$

where j denotes the j th sample, Δt denotes the sampling interval, $\tau_1 = R_{pa} C_{pa}$, and $\tau_2 = R_{pb} C_{pb}$.

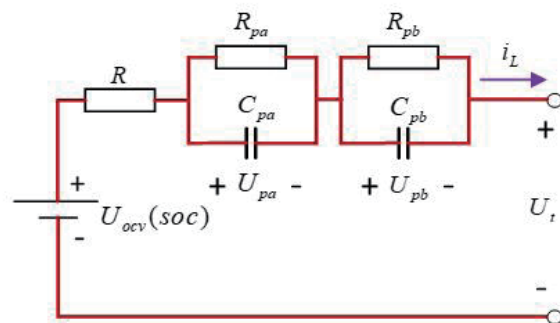


Fig. 1. (Color online) SO RC model.

The SO RC model can solve the problem of unsynchronized electrochemical polarization and concentration polarization processes, it can also better reflect the dynamic characteristics of the battery, enabling it to cope with relatively complex battery operating conditions.

3.2 ISO RC model

Although the SO RC model better considers the effect of polarization reflection on the dynamic characteristics of the battery, the hysteresis effect is still not considered. The hysteresis effect exhibits a complex dynamic behavior, which is reflected by the fact that the battery has different equilibrium potentials depending on whether it is previously charged or discharged, even if its SOC is the same.

The relationship between the hysteresis voltage and SOC due to the battery hysteresis effect is shown in Fig. 2 (obtained from the OCV–SOC curve in Sect. 5 after eliminating the battery polarization effect).

As seen in Fig. 2, the hysteresis voltage exists for different SOC of the battery, causing the same SOC to correspond to different OCVs when the battery is charged and discharged, thus affecting the accuracy of the battery model. Therefore, in this study, we propose a correction strategy to weaken the hysteresis effect and thus reduce its impact on the model accuracy. The hysteresis voltage–SOC curve is segmented and linearized into five segments in accordance with the curve characteristics, as shown in Fig. 3.

The linearized hysteresis voltage–SOC curve is described in the following form:

$$W(soc) = \begin{cases} A \cdot soc + B, & 0 \leq soc < 0.1 \\ C \cdot soc + D, & 0.1 \leq soc < 0.35 \\ P, & 0.35 \leq soc < 0.75, \\ E \cdot soc + F, & 0.75 \leq soc < 0.95 \\ G \cdot soc + H, & 0.95 \leq soc \leq 1 \end{cases} \quad (4)$$

where $A, B, C, D, E, F, G, H,$ and P are fitted parameters.

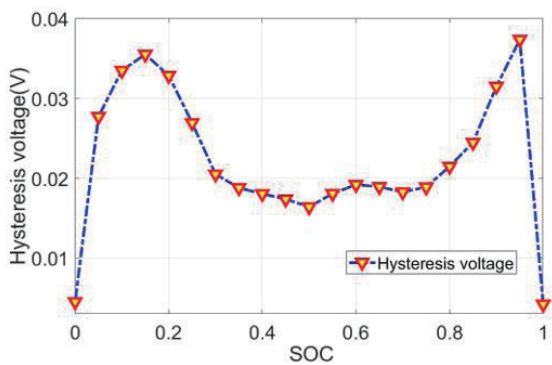


Fig. 2. (Color online) Hysteresis voltage–SOC curve.

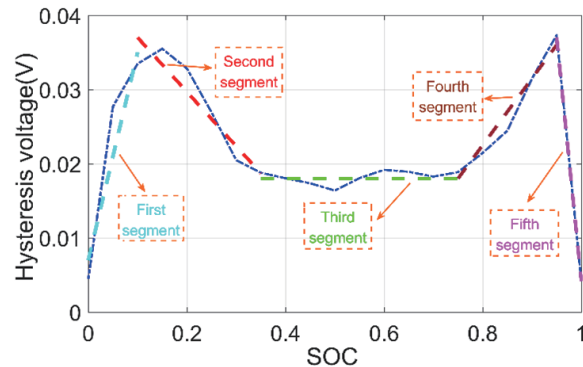


Fig. 3. (Color online) Segmented curve of hysteresis voltage after linearization.

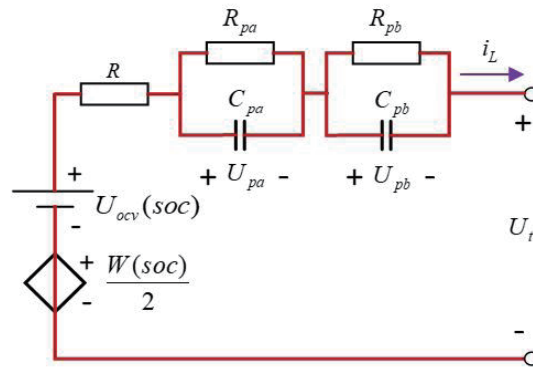


Fig. 4. (Color online) ISO RC model.

$\frac{W(soc)}{2}$ is introduced into the SO RC model as a correction to the average OCV–SOC curve in the form of a controlled voltage source, as shown in Fig. 4.

From Fig. 4, the expression for the terminal voltage of the model is derived as

$$U_t = U_{ocv}(soc) - R \cdot i_L - U_{pa} - U_{pb} + Sig \cdot \frac{W(soc)}{2}, \quad (5)$$

where Sig is the signal factor: $Sig = 1$ when $i_L > 0$, $Sig = -1$ when $i_L < 0$, and Sig is the same as its value at the previous sampling point when $i_L = 0$. The discretized expressions of U_{pa} and U_{pb} are the same as Eqs. (2) and (3), respectively.

The ISO RC model considers the hysteresis effect of the battery on the basis of the original model, which has higher accuracy in dealing with the battery dynamics and is more suitable for complex battery working conditions. Therefore, the ISO RC model is chosen for parameter identification in this study, and the accuracy and adaptability of the improved model are verified in Sect. 5.

4. Algorithm Analysis and Improvement

4.1 BMO

The BMO is a metaheuristic algorithm inspired by the mating behavior of barnacles in nature. The mating population of a barnacle includes all barnacles within its penile range and all barnacles that are beyond the penile range, but these barnacles may become competitors for its mate. Taking this concept as an inspiration, the barnacle algorithm is divided into the following stages.

4.1.1 Population initialization

Barnacles are considered as candidate solutions in the BMO and their population vectors can be described by the following $N \times n$ matrix:

$$X = \begin{pmatrix} x_1^1 & \cdots & x_1^N \\ \vdots & \ddots & \vdots \\ x_n^1 & \cdots & x_n^N \end{pmatrix}, \quad (6)$$

where N denotes the number of decision variables and n denotes the number of barnacles in the barnacle population. The upper and lower bounds of each decision variable are determined as follows:

$$ub = [ub_1, \dots, ub_i], \quad (7)$$

$$lb = [lb_1, \dots, lb_i], \quad (8)$$

where ub and lb respectively denote the upper and lower bounds of the i th decision variable. The algorithm is executed by first determining the value of each individual solution, and then placing the optimal solution at the top position of the matrix X by ranking the values of the individual solutions.

4.1.2 Algorithm selection process

The process of BMO selection was inspired by the selection of mates by barnacles, and the following criteria were followed in the selection process.

- (1) Selection is restricted to the length of the barnacle penis (pl), while the entire selection process is randomized.
- (2) Each barnacle can offer or receive sperm during fertilization but can only receive sperm from another barnacle once.
- (3) Although individual barnacles contain both female and male sexual organs, their self-fertilization process is not considered and no new offspring are produced by self-fertilization.
- (4) When all selections during the iterative process exceed the value of pl set by the previous initialization, the limit is exceeded and no normal mating process occurs, which also leads to the sperm-casting process.

Criteria (1) and (2) correspond to the mining process of the algorithm, while criterion (4) corresponds to the exploration process. Barnacles choose mates randomly, and thus the following equations are satisfied:

$$b_d = \text{randperm}(n), \quad (9)$$

$$b_m = \text{randperm}(n), \quad (10)$$

where n is the number of barnacle populations and b_d and b_m represent the mating of two barnacles.

4.1.3 Algorithm reproduction process

The process of BMO reproduction is mainly based on the Hardy–Weinberg principle. This leads to the following expression for the generation of new variables in barnacles:

$$x_i^{N_{new}} = px_{b_d}^N + qx_{b_m}^N, \quad (11)$$

where P denotes a pseudo-random number between 0 and 1 and $q = (1 - p)$. $x_{b_d}^N$ denotes the father parameter of the barnacle, and the corresponding $x_{b_m}^N$ denotes the mother parameter of the barnacle.

When the selected distance exceeds a predetermined pl value, a sperm-casting process occurs, expressed as follows:

$$x_i^{n_{new}} = rand \times x_{b_m}^n, \quad (12)$$

where $rand$ denotes a random number between 0 and 1. During each iteration, the optimal solution is selected and placed at the top of matrix X .

4.2 IBMO

Although the BMO has played an important role in some optimization problems, it has limitations: there is insufficient population diversity at the beginning of the iteration, it easily falls into a local optimum, and there is scope to improve the convergence accuracy and convergence speed. To address some of these shortcomings, the following improvement strategies are introduced in this study.

4.2.1 Tent chaos mapping

The quality of the initial population has a strong impact on the search efficiency of the BMO. In this study we take advantage of the regularity and ergodicity of tent chaos mapping and use it to generate the initial population of barnacles.

The tent chaos mapping equation is

$$Tent_{i+1} = \begin{cases} \frac{Tent_i}{0.7}, & rand < 0.7 \\ (1 - Tent_i) \times \frac{10}{3}, & rand \geq 0.7 \end{cases}. \quad (13)$$

Thus, the $n \times N$ population generation process for barnacles is as follows: an n -dimensional $rand$ vector is first generated as the first column of the population, after which the remaining

$N - 1$ columns of n -dimensional individuals are obtained by iterating over the individuals of each dimension using Eq. (13) and are then mapped to individual barnacles by the following equation:

$$X = Tent * (ub - lb) + lb, \quad (14)$$

where $Tent$ is the $n \times N$ -dimensional matrix obtained by iterating the above population generation process, X is the generated population, ub is the upper limit of individuals, and lb is the lower limit of individuals.

4.2.2 Cosine control factor

The cosine control factor possesses the oscillatory property of the cosine function and has good convergence, which can effectively improve the search range of the algorithm. Its equation is as follows:

$$cc_l = 0.5 \times \cos\left(\frac{l}{Iteration_max}\right) + 0.5, \quad (15)$$

where $Iteration_max$ is the maximum number of iterations and l is the current number of iterations.

Applying the cosine factor to Eq. (11) yields the new offspring equation

$$x_i^{N_{new}} = cc_i x_{b_d}^N + (1 - cc_i) x_{b_m}^N. \quad (16)$$

4.2.3 Levy flight strategy

To improve the performance of the algorithm by preventing it from falling into a local optimum, the Levy flight strategy (LF) is introduced in this study. The LF can effectively improve the search ability of the algorithm by random wandering. Its equation is expressed as follows:

$$Levy(\beta) \sim \frac{\sigma \times A}{|B|^{\frac{1}{\beta}}} \quad (17)$$

$$\sigma = \left[\frac{\sin(\pi \times \beta / 2)}{2^{(\beta-1)/2} \times \beta} \times \frac{\Gamma(1+\beta)}{\Gamma\left(\frac{1+\beta}{2}\right)} \right]^{\frac{1}{\beta}}, \quad (18)$$

where $Levy(\beta)$ is the random step, A and B are random numbers obeying the standard normal distribution, Γ is the gamma function, and β is the LF parameter, which is taken as 1.5 here.

By introducing the above LF into the BMO sperm-casting process, a new sperm-casting equation can be obtained as

$$x_i^{n_{new}} = Levy \times x_{b_m}^n, \quad (19)$$

where $Levy$ is a random search vector obeying the LF distribution.

4.2.4 IBMO operation process

The specific operation process of the IBMO is as follows.

- (1) Initialize parameters: set parameters such as the barnacle population size, the maximum number of iterations of the algorithm, pl values, ub , lb , and population dimensions.
- (2) Generate a more uniformly distributed initial population of barnacles using tent chaos mapping.
- (3) Calculate the initial fitness value of the barnacles, rank the barnacles in accordance with the fitness value, and place the optimal liberation at the top position of the matrix X .
- (4) Select male and female barnacles to be mated in accordance with the barnacle algorithm selection criterion.
- (5) Determine whether the distance between male and female barnacles is less than pl . When the distance is less than or equal to pl , the reproduction process of barnacles occurs in combination with the cosine control factor to update the position of the next generation; otherwise, the sperm-casting process occurs in combination with the LF to update the position of the offspring.
- (6) Calculate the fitness value of the offspring barnacles and rank them to update the optimal solution at the top position of X .
- (7) Determine whether the end-of-iteration condition is satisfied. If the condition is satisfied, the optimal solution is output; otherwise, return to step 4 to continue the iterative process.

The flowchart of the IBMO operation is shown in Fig. 5 (improvements have been marked in light green).

4.3 Algorithm performance testing

Nine standard test functions were selected to test the performance of the IBMO. Among them, F_1 – F_5 are single-peak test functions, which were used to test the local search capability of the algorithm, and F_6 – F_9 are multi-peak test functions, which were used to test the global search capability of the algorithm. The information of each test function is shown in Table 1.

To further validate the superiority of the IBMO, we tested the PSO,⁽²⁵⁾ the whale optimization algorithm (WOA),⁽²⁶⁾ the seagull optimization algorithm (SOA),⁽²⁷⁾ the sailfish optimizer (SFO),⁽²⁸⁾ the grey wolf optimizer (GWO),⁽²⁹⁾ the improved grey wolf optimizer (IGWO),⁽³⁰⁾ and

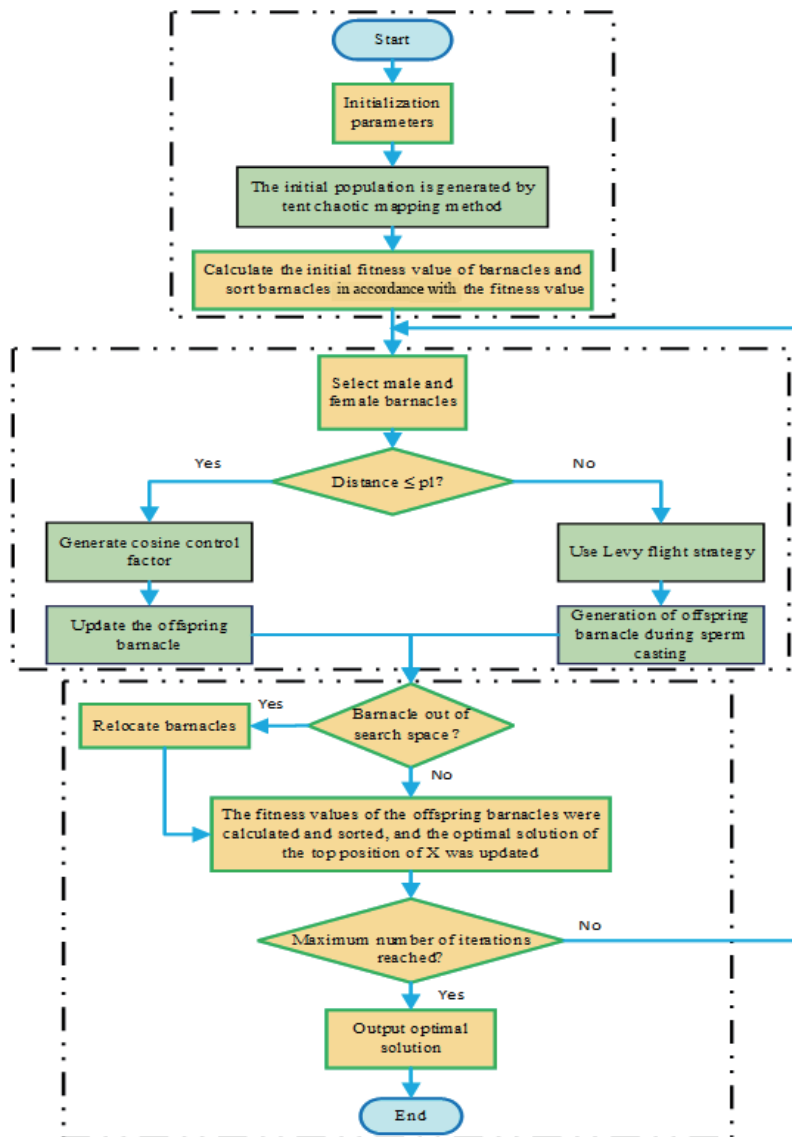


Fig. 5. (Color online) IBMO operation flow chart.

the conventional BMO algorithm for comparison. All algorithms were tested using MATLAB R2017a, the computer operating system was Windows 10, the processor was Intel Core i5-6300HQ 12 GB, the population was set to 30 for all algorithms, the maximum number of iterations was set to 500, and the other parameters of the algorithms were consistent with the original literature. Each algorithm was run 30 times independently for each standard test function, and the optimal value, average value, standard deviation, and average rank of the algorithm were recorded for the 30 results, The test results are shown in Table 2.

As can be seen from Table 2, the IBMO has the best performance among the eight tested algorithms in solving four of the single-peak test functions F_1 , F_2 , F_4 , and F_5 . It is thus demonstrated that the IBMO has excellent local search ability with a significantly better

Table 1
Information of each test function,

Classification	Test function	Dim	Optimum value	Range
Single-peak test functions	$F_1 = \sum_{i=1}^n x_i^2$	30	0	[-100, 100]
	$F_2 = \prod_{i=1}^n x_i + \sum_{i=1}^n x_i $	30	0	[-10, 10]
	$F_3 = \sum_{i=1}^n ([x_i + 0.5])^2$	30	0	[-100, 100]
	$F_4 = \max_i \{ x_i , 1 \leq i \leq n\}$	30	0	[-100, 100]
	$F_5 = \sum_{i=1}^n ix_i^4 + \text{random}[0,1)$	30	0	[-1.28, 1.28]
	$F_6 = \sum_{i=1}^n \frac{x_i^2}{4000} - \prod_{i=1}^n \cos(\frac{x_i}{\sqrt{i}}) + 1$	30	0	[-600, 600]
	$F_7 = \sum_{i=1}^n (x_i^2 - 10 * \cos(2\pi x_i) + 10n)$	30	0	[-5.12, 5.12]
	$F_8 = -20 * \exp(-0.2 * \sqrt{\frac{1}{n} \sum_{i=1}^n x_i^2}) - \exp(\frac{1}{n} \sum_{i=1}^n \cos(2\pi x_i)) + 20 + e$	30	0	[-32, 32]
Multipeak test functions	$F_9 = \frac{\pi}{n} \left\{ \begin{array}{l} 10 \sin(\pi y_1) + (y_n + 1)^2 + \\ \sum_{i=1}^{n-1} (y_i - 1)^2 [10 \sin^2(\pi y_i + 1) + 1] \end{array} \right\}$ $+ \sum_{i=1}^n u(x_i, 10, 100, 4);$ $y_i = 1 + \frac{x_i + 1}{4}, u(x_i, a, k, m) = \begin{cases} k(x_i - a)^m, & x_i > a \\ 0, & -a < x_i < a \\ k(-x_i - a)^m, & x_i < -a \end{cases}$	30	0	[-50, 50]

convergence effect than other algorithms. The IBMO is also effective in solving the four multipeaked test functions F_6 – F_9 . Except for the second ranking in solving F_9 , the IBMO ranks first among the eight tested algorithms in solving the multipeak test functions. This demonstrates that the IBMO has excellent global search ability and avoids local optima.

To further demonstrate the convergence performance of each algorithm, Fig. 6 illustrates the convergence curves of each algorithm when solving F_1, F_4, F_5, F_6, F_7 , and F_8 .

It can be seen that the IBMO has a higher convergence speed and convergence accuracy than the other algorithms, which demonstrates that the IBMO has relatively stable and excellent convergence performance.

5. Experimental Case Study Based on IBMO

We conducted experiments with 18650 type ternary LIB data, whose rated capacity is 2000 mAh, rated voltage is 3.7 V, and charge/discharge cutoff voltages are 4.2 and 2.5 V, respectively.

Table 2
Algorithm test results.

Function	Statistical value	PSO	WOA	SOA	SFO	GWO	IGWO	BMO	IBMO
F_1	Optimum value	3.29E-06	2.58E-87	1.09E-13	1.29E-13	5.40E-30	8.72E-96	0.00E+00	0.00E+00
	Average value	1.19E-04	1.60E-73	1.44E-11	6.71E-11	1.55E-27	6.37E-92	0.00E+00	0.00E+00
	Standard deviation	1.37E-04	6.20E-73	3.54E-11	7.69E-11	2.95E-27	3.33E-91	0.00E+00	0.00E+00
	Rank	8	4	6	7	5	3	1	1
F_2	Optimum value	3.83E-03	4.80E-58	2.37E-09	6.57E-06	1.22E-17	1.82E-52	2.50E-307	0.00E+00
	Average value	3.59E-02	2.37E-51	1.87E-08	3.85E-05	9.85E-17	3.48E-51	1.37E-284	0.00E+00
	Standard deviation	4.44E-02	8.82E-51	1.53E-08	3.21E-05	9.42E-17	7.83E-51	0.00E+00	0.00E+00
	Rank	8	3	6	7	5	4	2	1
F_3	Optimum value	1.05E-05	1.47E-01	2.33E+00	5.12E-08	2.23E-01	2.00E+00	1.34E-01	1.29E-01
	Average value	1.14E-04	4.33E-01	3.24E+00	1.41E-02	7.41E-01	2.85E+00	5.69E-01	5.36E-01
	Standard deviation	1.13E-04	2.35E-01	5.44E-01	4.45E-02	3.53E-01	3.73E-01	2.85E-01	2.73E-01
	Rank	1	3	8	2	6	7	5	4
F_4	Optimum value	7.50E-01	4.10E-01	1.85E-05	9.08E-08	6.01E-08	2.13E-37	2.01E-306	0.00E+00
	Average value	1.09E+00	5.28E+01	4.25E-03	1.29E-06	7.66E-07	5.81E-35	1.66E-285	0.00E+00
	Standard deviation	2.11E-01	2.51E+01	7.76E-03	1.38E-06	1.20E-06	2.42E-34	0.00E+00	0.00E+00
	Rank	7	8	6	5	4	3	2	1
F_5	Optimum value	6.79E-02	4.28E-05	4.71E-04	1.53E-05	6.98E-04	1.11E-05	2.21E-07	1.56E-08
	Average value	1.69E-01	4.70E-03	3.00E-03	6.03E-04	1.63E-03	3.49E-04	3.68E-05	2.83E-05
	Standard deviation	6.08E-02	6.91E-03	2.13E-03	4.72E-04	7.60E-04	2.68E-04	3.26E-05	2.19E-05
	Rank	8	7	6	4	5	3	2	1
F_6	Optimum value	1.33E-06	0.00E+00	1.10E-13	2.12E-15	0.00E+00	0.00E+00	0.00E+00	0.00E+00
	Average value	5.86E-03	3.87E-03	2.01E-02	3.52E-12	6.53E-03	1.46E-03	0.00E+00	0.00E+00
	Standard deviation	1.03E-02	2.12E-02	2.92E-02	5.71E-12	1.17E-02	4.74E-03	0.00E+00	0.00E+00
	Rank	6	5	8	3	7	4	1	1
F_7	Optimum value	2.52E+01	0.00E+00	3.41E-13	3.21E-11	6.73E-14	0.00E+00	0.00E+00	0.00E+00
	Average value	5.68E+01	0.00E+00	2.10E+00	5.02E-07	3.54E+00	0.00E+00	0.00E+00	0.00E+00
	Standard deviation	1.54E+01	0.00E+00	4.40E+00	7.96E-07	4.50E+00	0.00E+00	0.00E+00	0.00E+00
	Rank	8	1	6	5	7	1	1	1
F_8	Optimum value	5.01E-03	8.88E-16	2.00E+01	1.86E-07	6.43E-14	4.23E-15	8.88E-16	8.88E-16
	Average value	2.68E-01	4.83E-15	2.00E+01	2.38E-06	2.23E-13	5.78E-15	8.88E-16	8.88E-16
	Standard deviation	5.32E-01	2.62E-15	1.40E-03	2.76E-06	1.42E-14	1.76E-15	4.36E-31	1.00E-31
	Rank	7	3	8	6	5	4	1	1
F_9	Optimum value	1.63E-07	2.02E-03	1.36E-01	6.63E-10	6.59E-03	1.25E-01	7.45E-03	6.68E-04
	Average value	1.04E-02	3.12E-02	3.12E-01	1.48E-02	4.99E-02	2.51E-01	1.83E-01	1.35E-02
	Standard deviation	3.16E-02	3.92E-02	1.30E-01	4.23E-02	2.99E-02	1.23E-01	4.11E-01	1.32E-02
	Rank	1	4	8	3	5	7	6	2

5.1 Acquisition of OCV–SOC relationship curve

There is a relatively stable relationship between SOC and OCV for the same battery, and an accurate OCV–SOC relationship is crucial in the battery identification process.⁽³¹⁾ Therefore, an accurate OCV–SOC relationship curve should be obtained first.

We start charging the battery in a thermostat at a multiplier current of 0.5 C. The OCV–SOC relationship at the time of charging is obtained by charging for 6 min at a time, followed by 2 h of resting until the charge cutoff voltage is reached. Similarly, the OCV–SOC relationship during discharge is obtained. Since the SOC value at each sampling point cannot be measured directly, the ampere-time integration method is used to calculate their values with the following equation:

$$SOC_{j+1} = SOC_j + \frac{\Delta t \cdot i_L}{C_N}, \quad (20)$$

where i_L denotes the battery charging and discharging current (positive when charging and negative when discharging), j denotes the j th sampling, Δt denotes the sampling interval, and C_N denotes the rated capacity of the battery.

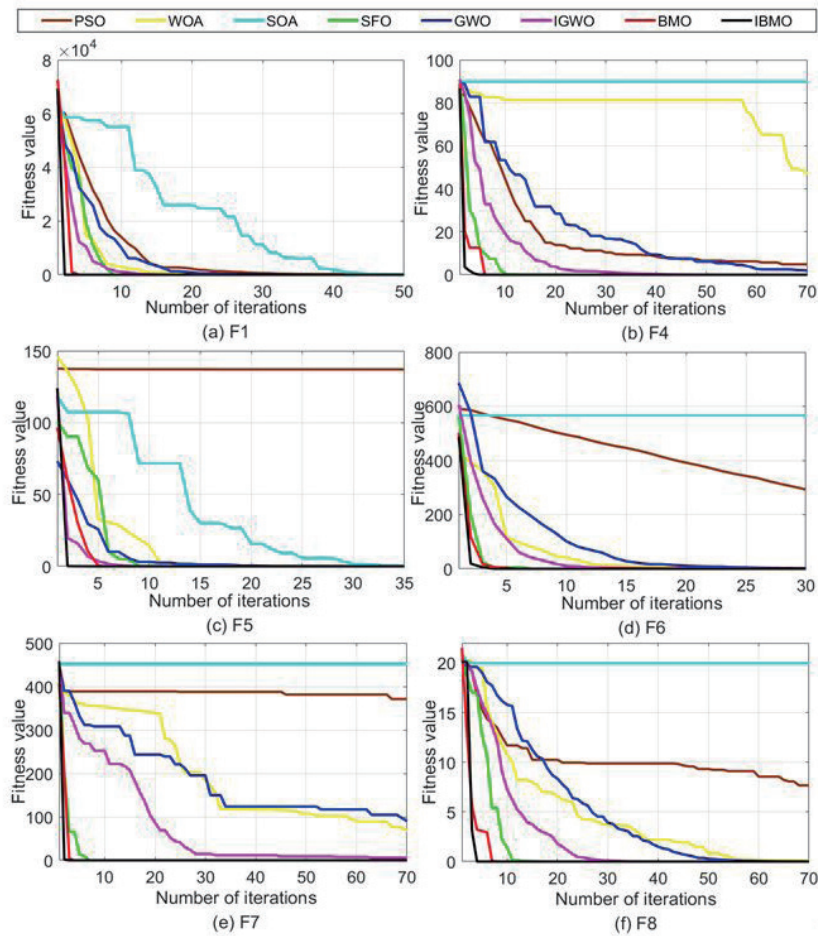


Fig. 6. (Color online) Algorithm convergence curves.

The charge/discharge OCV–SOC relationship for each sampling point is fitted using a seventh-order polynomial with the following equation:

$$U_{ocv}(soc) = a_7 \cdot soc^7 + a_6 \cdot soc^6 + a_5 \cdot soc^5 + a_4 \cdot soc^4 + a_3 \cdot soc^3 + a_2 \cdot soc^2 + a_1 \cdot soc + a_0. \quad (21)$$

The charge and discharge OCV–SOC fitting curves and their average curve are considered to approximate the actual battery, and the three curves are illustrated in Fig. 7.

5.2 Acquisition of battery operating conditions data

After resting the battery for 2 h, charge and discharge experiments were performed on it, and the whole experimental process was carried out in a constant-temperature chamber. The resulting battery data under two operating conditions are shown in Figs. 8 and 9. The first condition is the parameter identification condition, in which parameter identification

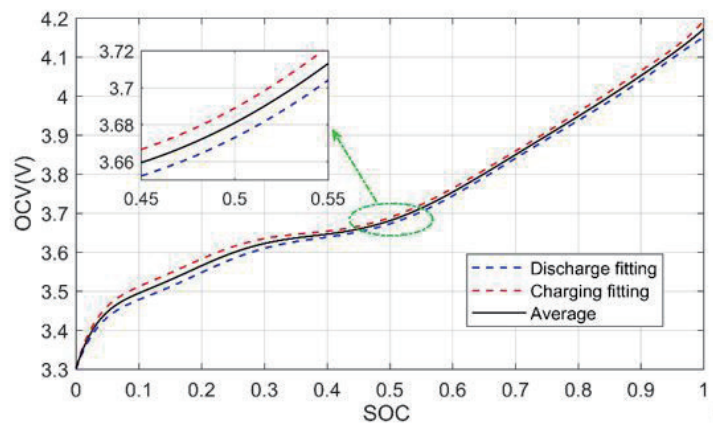


Fig. 7. (Color online) OCV–SOC fitting curves and their average curve.

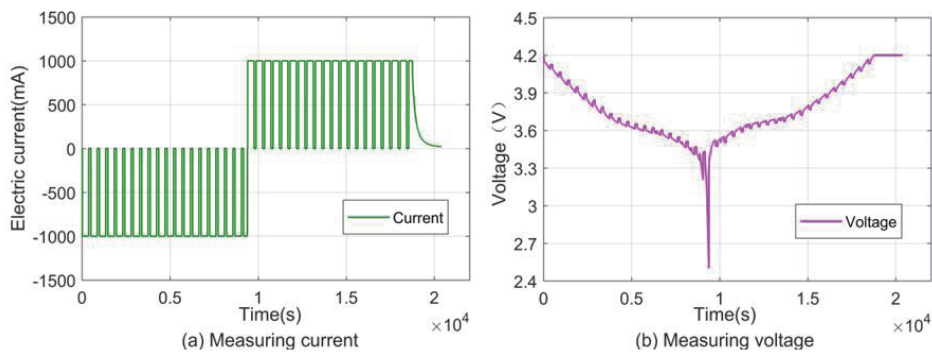


Fig. 8. (Color online) Parameter identification condition.

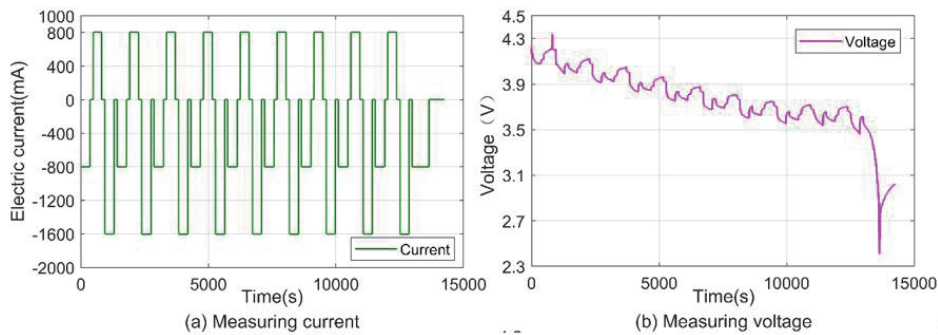


Fig. 9. (Color online) Verification condition.

experiments are conducted to verify the identification performance of the algorithm. The other condition is the validation condition, which is used to verify that the ECM of the battery after parameter identification is also applicable to other conditions. In Figs. 8 and 9, (a) shows the current data of battery charging and discharging and (b) shows the battery terminal voltage data measured during battery charging and discharging.

5.3 Parameter identification process

The root mean square error (*RMSE*) can better reflect the error between the identified value and the actual value; thus, the *RMSE* of voltage is chosen as the fitness value function of the IBMO in this study, with the fitness expressed as

$$Fitness = \sqrt{\frac{1}{Z} \cdot \sum_{k=1}^Z (U_m^{(k)} - U_t^{(k)})^2}, \quad (22)$$

where $U_m^{(k)}$ is the k th measured voltage, $U_t^{(k)}$ is the k th simulated voltage, and Z is the total number of samples.

The IBMO-based parameter identification process is as follows.

- (1) Input the discriminated working current data and the actual measured voltage data matched with it.
- (2) Obtain the SOC data and the OCV curve corresponding to the SOC through the OCV–SOC curve by the ampere-time integration method.
- (3) Import the current, voltage, SOC, OCV, and the mathematical expressions for the ISO RC model into the IBMO, and iteratively optimize the model parameters by the IBMO to identify parameters including R , R_{pa} , R_{pb} , C_{pa} , and C_{pb} .
- (4) Output the model parameter identification results of the IBMO.

5.4 Experimental results and analysis

The BMO and IBMO were used for parameter identification for the ISO RC model under the identification condition (Fig. 8), whereas the LS, PSO, and BMO were used for parameter identification of the ordinary SO RC under the same conditions as in the control experiments. The obtained parameter identification results are shown in Table 3.

The parameter identification results of the five models shown in Table 3 are simulated for the operating conditions shown in Fig. 8, and the voltage simulation results are shown in Fig. 10. From Fig. 10, for the BMO algorithm, the simulated voltage of the BMO-ISO RC model (red line) is closer to the real value (black line) than that of the BMO-SO RC model (green line), which demonstrates that the ISO RC model can better reflect the actual operation of the LIB and the

Table 3
Parameter identification results of each model.

Model	Parameter				
	R	R_{pa}	R_{pb}	C_{pa}	C_{pb}
LS-SO RC	0.0285	0.0395	0.0412	28.63	415.76
PSO-SO RC	0.0356	0.0322	0.0485	33.14	390.87
BMO-SO RC	0.0334	0.0023	0.0503	43.31	488.57
BMO-ISO RC	0.0316	0.0399	0.0401	30.23	469.93
IBMO-ISO RC	0.0301	0.0347	0.0434	20.00	377.04

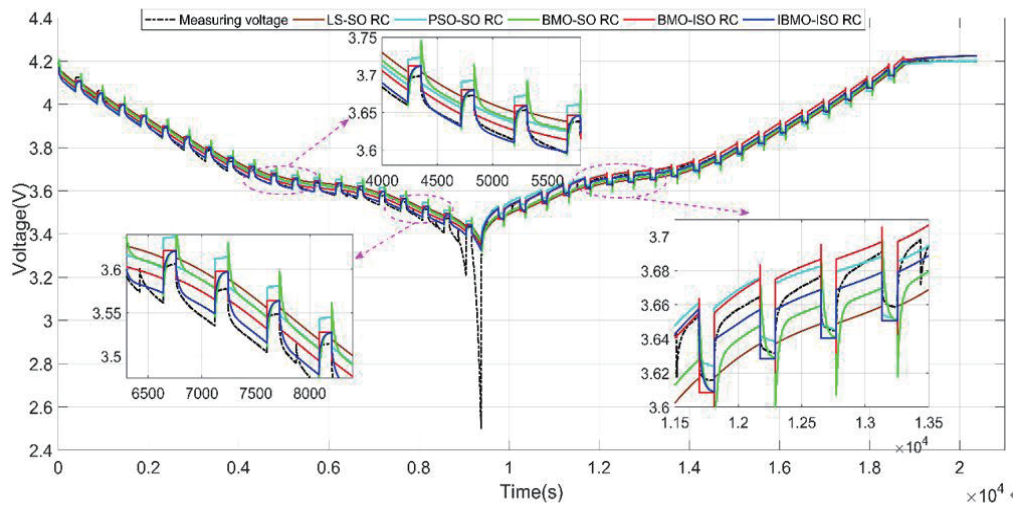


Fig. 10. (Color online) Voltage simulation results of the models.

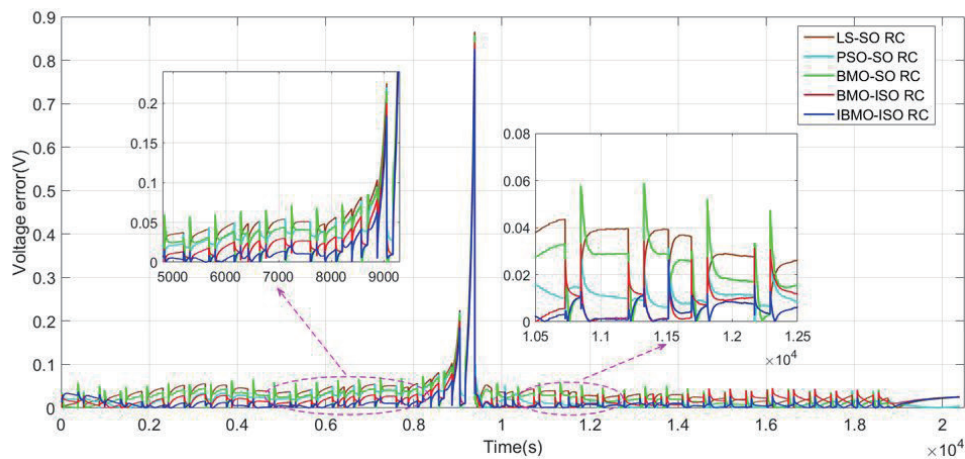


Fig. 11. (Color online) Voltage simulation errors for the five models.

validity of the correction to the model in Sect. 3. Moreover, the simulated voltage of the IBMO-ISO RC model (blue line) is closest to the real value, indicating that it has the best simulation performance and can better simulate the operating characteristics of LIBs than the other models, thus demonstrating the effectiveness of the improved algorithm and model in this study.

The voltage error values between the simulated output voltage and the actual measured voltage for the five models are shown in Fig. 11. The voltage error of the IBMO-ISO RC model is the smallest, followed by that of the BMO-ISO RC model.

$RMSE$, R-square (R^2), mean absolute percentage error ($MAPE$), and cumulative error (CE) were used to evaluate the performance of the models. $RMSE$ and $MAPE$ can better reflect the degree of deviation of the simulated voltage from the actual measured voltage; the smaller their values, the smaller the deviation of the simulated voltage. R^2 reflects the degree of fit between

the model simulation curve and the actual measured curve. If R^2 is close to 1, the fit is good, and if R^2 is close to 0, the fit is poor. CE reflects the overall effectiveness of the simulation. The smaller its value, the greater the overall effectiveness of the simulation of the model. The expressions for the above errors are below. The errors of each model for the identified working conditions are shown in Table 4.

$$RMSE = \sqrt{\frac{1}{Z} \cdot \sum_{k=1}^Z (U_m^{(k)} - U_t^{(k)})^2} \quad (23)$$

$$R^2 = 1 - \frac{\sum_{k=1}^Z (U_m^{(k)} - U_t^{(k)})^2}{\sum_{k=1}^Z (U_m^{(k)} - \overline{U_t^{(k)}})^2} \quad (24)$$

$$MAPE = \frac{100\%}{Z} \cdot \sum_{k=1}^Z \left| \frac{U_t^{(k)} - U_m^{(k)}}{U_m^{(k)}} \right| \quad (25)$$

$$CE = \sum_{k=1}^Z |U_m^{(k)} - U_t^{(k)}| \quad (26)$$

Here, $\overline{U_t^{(k)}}$ denotes the mean value of $U_t^{(k)}$ and other variables have the same meaning as in Eq. (22).

Table 4 shows that the $RMSE$ and $MAPE$ values of the BMO-ISO RC model are smaller than those of the BMO-SO RC model, the R^2 value is closer to 1 than that of the BMO-SO RC model, and the CE value is only 397.85. This demonstrates that after considering the hysteresis effect of the LIB, the ISO RC model can reflect the operating characteristics of an LIB more accurately than the SO RC model and has a greater recognition effectiveness. All four error evaluations of the IBMO-ISO RC model are optimal, with the lowest $RMSE$ and $MAPE$ values of 0.0431 and 0.38%, respectively. This indicates that the IBMO-ISO RC model has the smallest deviation between the simulated voltage and the actual measured voltage. Its R^2 value is 0.9686, which is the closest to 1 among the five models, indicating that its voltage simulation curve most closely

Table 4
Model errors under identification condition.

Model	Error type			
	$RMSE$	R^2	$MAPE$	CE
LS-SO RC	0.0547	0.9495	0.85%	615.27
PSO-SO RC	0.0495	0.9587	0.60%	427.81
BMO-SO RC	0.0514	0.9555	0.72%	519.90
BMO-ISO RC	0.0467	0.9634	0.55%	397.85
IBMO-ISO RC	0.0431	0.9686	0.38%	265.89

fits the actual curve. Meanwhile, its CE value is only 265.89, which is the smallest among all models, demonstrating that the overall simulation effectiveness of the IBMO-ISO RC model has been greatly improved compared with the other models and the effectiveness of the improved algorithm and model.

The parameters obtained from the IBMO-ISO RC model identification are kept constant while the validation current shown in Fig. 9 is input. Figures 12 and 13 show the voltage simulation results and the error voltage of the model under the validation condition, respectively.

As seen in Figs. 12 and 13, the model maintains high simulation accuracy even though the working current has changed. In the SOC interval of [0.2, 1], the error is mostly less than 0.04 V, as expected, although the error is larger when the SOC is less than 0.2. Under the validation condition, the model maintains high stability and accuracy. This indicates that for the same battery, the parameters obtained by the IBMO-ISO RC model from one working condition are applicable to other working conditions of this battery, which demonstrates the generality of the model. The simulation voltage errors for each model under the validation condition are shown in Table 5.

As shown in the table, the simulation error of the IBMO-ISO RC model remains at a low value as the working current changes. Its $RMSE$ and $MAPE$ values are 0.0483 and 0.56%, respectively, which are the smallest among the five models. Moreover, its R^2 is closest to 1, indicating the closest fitting. Its CE is reduced by 326.98, 211.45, 271.25, and 138.86, respectively, compared with the other four models, thus indicating the improvement of overall simulation results.

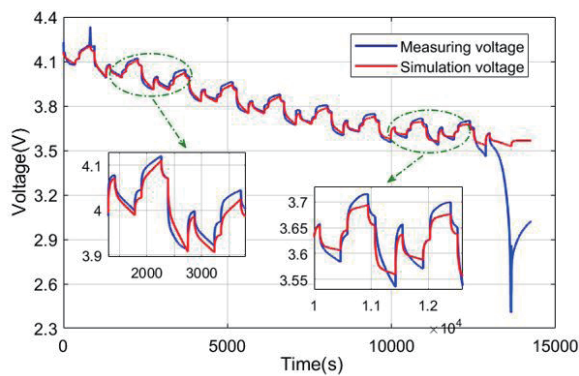


Fig. 12. (Color online) Simulation results of the model under the validation condition.

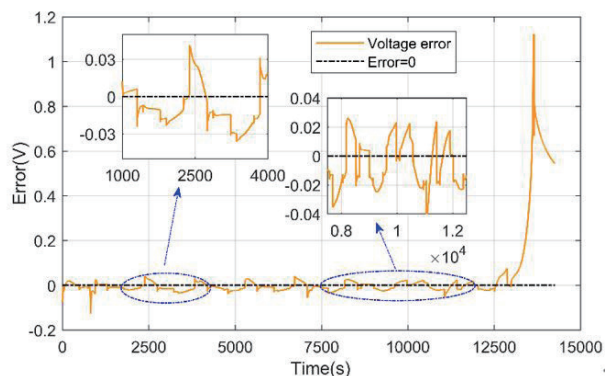


Fig. 13. (Color online) Model simulation error under the validation condition.

Table 5
Model errors under validation condition.

Model	Error type			
	$RMSE$	R^2	$MAPE$	CE
LS-SO RC	0.0642	0.9112	0.96%	637.84
PSO-SO RC	0.0587	0.9311	0.84%	522.31
BMO-SO RC	0.0612	0.9224	0.91%	582.11
BMO-ISO RC	0.0531	0.9385	0.75%	443.25
IBMO-ISO RC	0.0483	0.9494	0.56%	310.86

The parameter identification method proposed in this study is competitive with methods in other studies. For example, He *et al.*⁽³²⁾ used PSO incorporating an adaptive optimization strategy for parameter identification of LIBs, and *MAPE* of the identification results was 1.5%. The recursive LS method used by Yang *et al.*⁽³³⁾ was applied to the experimental data in this study, and the *RMSE* value was 0.0473. Ling and Wei⁽³⁴⁾ used an adaptive genetic algorithm to identify the model parameters offline, and the *RMSE* value was 0.0490. Peng *et al.*⁽³⁵⁾ used an improved adaptive dual traceless Kalman filter algorithm for battery model parameter estimation, and its error band was controlled at 2.8%, whereas the error band of the proposed method in this study was controlled at less than 1%. Compared with the parameter identification methods reported elsewhere, our proposed method is competitive according to the results of our analysis of the error evaluation index, thus demonstrating its accuracy and effectiveness.

6. Conclusion

The work carried out in this study is summarized as follows.

- (1) We propose the IBMO by introducing tent chaos mapping, the cosine control factor, and Levy flight strategy into the BMO. The IBMO effectively solves the problem of the BMO tending to fall into a local optimum and it also has better convergence performance.
- (2) We propose an ISO RC model, which can better cope with complex battery conditions with higher accuracy.
- (3) We establish an IBMO-ISO RC parameter identification model based on the IBMO. The simulation effect of the IBMO-ISO RC model is verified for two working conditions, and the results show that the IBMO-ISO RC model has higher simulation accuracy and stability than the other models used for comparison, with *RMSE* of only 0.0431 and 0.0483 and *MAPE* of only 0.38 and 0.56% for the two conditions.
- (4) The proposed IBMO algorithm can be applied not only to the LIB parameter identification problem, but also to other optimization problems, for example, the model parameter identification of sensors and some optimization problems in the field of sensors.

The proposed IBMO algorithm still fails to converge all test functions to the global optimum, and there is scope to improve its convergence performance. In future research, we will focus on addressing this limitation. For example, the algorithm can be further improved to model the characteristics of a sensor to improve its effectiveness for sensor model parameter identification.

References

- 1 H. C. Li, D. Yang, H. J. Cao, W. W. Ge, E. H. Chen, X. H. Wen, and C. B. Li: *Energy* **239** (2022) 122178. <https://doi.org/10.1016/j.energy.2021.122178>
- 2 Y. Li, K. L. Liu, A. M. Foley, A. Zulke, M. Bercibar, E. Nanini-Maury, J. Van Mierlo, and H. E. Hoster: *Renewable Sustainable Energy Rev.* **113** (2019) 109254. <https://doi.org/10.1016/j.rser.2019.109254>
- 3 Y. Zhao, P. Stein, Y. Bai, M. Al-Siraj, Y. Y. W. Yang, and B. X. Xu: *J. Power Sources* **413** (2019) 259. <https://doi.org/10.1016/j.jpowsour.2018.12.011>
- 4 X. Lai, Y. J. Zheng and, T. Sun: *Electrochim. Acta* **259** (2018) 566. <https://doi.org/10.1016/j.electacta.2017.10.153>
- 5 Y. Li, M. Vilathgamuwa, T. Farrell, S. S. Choi, N. T. Tran, and J. Teague: *Electrochim. Acta* **299** (2019) 451. <https://doi.org/10.1016/j.electacta.2018.12.167>

- 6 T. Kalogiannis, M. S. Hosen, M. A. Sokkeh, S. Goutam, J. Jaguemont, L. Jin, G. Qiao, M. Berecibar, and J. V. Mierlo: *Energies* **12** (2019) 4031. <https://doi.org/10.3390/en12214031>
- 7 Y. Hu and S. Yurkovich: *J. Power Sources* **196** (2011) 2913. <https://doi.org/10.1016/j.jpowsour.2010.10.072>
- 8 T. C. Ouyang, P. H. Xu, J. X. Chen, J. Lu, and N. Chen: *Electrochim. Acta* **353** (2020) 136576. <https://doi.org/10.1016/j.electacta.2020.136576>
- 9 L. L. Li, Z. F. Liu, M. L. Tseng, S. J. Zheng, and M. K. Lim: *Appl. Soft Comput.* **108** (2021) 107504. <https://doi.org/10.1016/j.asoc.2021.107504>
- 10 Z. F. Liu, L. L. Li, Y. W. Liu, J. Q. Liu, H. Y. Li, and Q. Shen: *Energy* **235** (2021) 121407. <https://doi.org/10.1016/j.energy.2021.121407>
- 11 M. H. Sulaiman, Z. Mustaffa, M. M. Saari, and H. Daniyal: *Eng. Appl. Artif. Intell.* **87** (2020) 103330. <https://doi.org/10.1016/j.engappai.2019.103330>
- 12 P. Z. Lyu, X. J. Liu, J. Qu, J. T. Zhao, Y. T. Huo, Z. G. Qu, and Z. H. Rao: *Energy Storage Mater.* **31** (2020) 195. <https://doi.org/10.1016/j.ensm.2020.06.042>
- 13 B. Y. Ren, C. X. Xie, X. D. Sun, Q. Zhang, and D. Yan: *IET Power Electron.* **13** (2020) 2531. <https://doi.org/10.1049/iet-pel.2019.1589>
- 14 G. L. Plett: *J. Power Sources* **134** (2004) 262. <https://doi.org/10.1016/j.jpowsour.2004.02.032>
- 15 N. A. Windarko, and J. Choi: *J. Power Electron.* **10** (2010) 181. <https://doi.org/10.6113/JPE.2010.10.2.181>
- 16 M. Verbrugge, and B. Koch: *J. Electrochem. Soc.* **153** (2006) A187. <https://iopscience.iop.org/article/10.1149/1.2128096>
- 17 B. Pattipati, C. Sankavaram, and K. R. Pattipati: *IEEE Trans. Syst. Man Cybern. Part C Appl. Rev.* **41** (2011) 869. <https://doi.org/10.1109/TSMCC.2010.2089979>
- 18 X. J. Tan, D. Zhan, P. X. Lyu, J. Rao, and Y. Q. Fan: *J. Power Sources* **484** (2021) 229233. <https://doi.org/10.1016/j.jpowsour.2020.229233>
- 19 J. Li, L. L. Zou, F. Tian, X. W. Dong, Z. Q. Zou, and H. Yang: *J. Electrochem. Soc.* **163** (2016) A1646. <https://iopscience.iop.org/article/10.1149/2.0861608jes>
- 20 W. J. Shen and H. X. Li: *Energies* **10** (2017) 432. <https://doi.org/10.3390/en10040432>
- 21 Z. H. Yu, L. J. Xiao, H. Y. Li, X. L. Zhu, and R. T. Huai: *IEEE Trans. Ind. Electron.* **64** (2017) 5690. <https://doi.org/10.1109/TIE.2017.2677319>
- 22 L. Li, H. R. Zhu, A. J. Zhou, M. H. Hu, C. Y. Fu, and D. T. Qin: *Int. J. Electrochem. Sci.* **15** (2020) 6863. <https://doi.org/10.1049/rpg2.12172>
- 23 R. A. El-Schiemy, M. A. Hamida, and T. Mesbahi: *Int. J. Hydrogen Energy* **45** (2020) 8833. <https://doi.org/10.1016/j.ijhydene.2020.01.067>
- 24 S. Ferahtia, A. Djeroui, H. Rezk, A. Chouder, A. Houari, and M. Machmoum: *Int. J. Energy Res.* **45** (2021) 16741. <https://doi.org/10.1002/er.6921>
- 25 C. A. C. Coello, G. T. Pulido, and M. S. Lechuga: *IEEE Trans. Evol. Comput.* **8** (2004) 256. <https://doi.org/10.1109/TEVC.2004.826067>
- 26 S. Mirjalili and A. Lewis: *Adv. Eng. Software* **95** (2016) 51. <https://doi.org/10.1016/j.advengsoft.2016.01.008>
- 27 G. Dhiman and V. Kumar: *Knowl. Based Syst.* **165** (2019) 169. <https://doi.org/10.1016/j.knosys.2018.11.024>
- 28 S. Shadravan, H. R. Naji, and V. K. Bardsiri: *Eng. Appl. Artif. Intell.* **80** (2019) 20. <https://doi.org/10.1016/j.engappai.2019.01.001>
- 29 S. Mirjalili, S. M. Mirjalili, and A. Lewis: *Adv. Eng. Software* **69** (2014) 46. <https://doi.org/10.1016/j.advengsoft.2013.12.007>
- 30 M. H. Nadimi-Shahraki, S. Taghian, and S. Mirjalili: *Expert Syst. Appl.* **166** (2021) 113917. <https://doi.org/10.1016/j.eswa.2020.113917>
- 31 Y. Z. Cui, P. J. Zuo, C. Y. Du, Y. Z. Gao, J. Yang, X. Q. Cheng, Y. L. Ma, and G. P. Yin: *Energy* **144** (2018) 647. <https://doi.org/10.1016/j.energy.2017.12.033>
- 32 M. F. He, S. L. Wang, C. Fernandez, C. M. Vu, X. X. Li, and E. D. Bobabee: *Int. J. Electrochem. Sci.* **16** (2021) 20. <https://doi.org/10.20964/2021.05.55>
- 33 K. Yang, Y. G. Tang, and Z. Zhang: *Energies* **14** (2021) 15. <https://doi.org/10.3390/en14041054>
- 34 L. Y. Ling, and Y. Wei: *IEEE Access* **9** (2021) 47588. <https://doi.org/10.1109/ACCESS.2021.3068813>
- 35 N. Peng, S. Z. Zhang, X. Guo, and X. W. Zhang: *Int. J. Energy Res.* **45** (2021) 975. <https://doi.org/10.1002/er.6088>

About the Authors



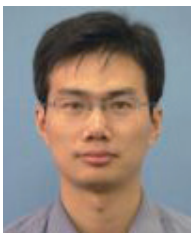
Jiarong Li received her B.S. degree in electrical engineering from Huaihai Institute of Technology in 1993 and her M.S. degree in power electronics and power transmission from Nanjing University of Aeronautics and Astronautics in 2001. Currently, she is an associate professor of the Electrical Engineering College, Yancheng Institute of Technology. Her current research interests are power systems and new energy systems. (lijr@ycit.cn)



Cheng-Jian Lin received his B.S. degree in electrical engineering from Ta Tung Institute of Technology, Taipei, Taiwan, R.O.C., in 1986 and his M.S. and Ph.D. degrees in electrical and control engineering from National Chiao Tung University, Taiwan, R.O.C., in 1991 and 1996, respectively. Currently, he is a chair professor of the Computer Science and Information Engineering Department, National Chin-Yi University of Technology, Taichung, Taiwan, R.O.C., and dean of Intelligence College, National Taichung University of Science and Technology, Taichung, Taiwan, R.O.C. His current research interests are machine learning, pattern recognition, intelligent control, image processing, intelligent manufacturing, and evolutionary robots. (cjlin@ncut.edu.tw)



Haiyu Wang received his M.S. degree from State Key Laboratory of Reliability and Intelligence of Electrical Equipment, Hebei University of Technology, Tianjin 300401, China, in 2022. His current research interests are machine learning, evolutionary computation, lithium-ion batteries, and electric vehicles. (202021401010@stu.hebut.edu.cn)



Jiarong Kan received his M.S. degree in electrical engineering from Nanjing University of Aeronautics and Astronautics (NUAA) in 2007. Currently, he is a professor of the School of Electrical Engineering, Yancheng Institute of Technology. He is the holder of seven patents and the author or coauthor of more than 40 technical papers. His current research interests include power electronics in renewable energy generation. (kanjr@163.com)